Res Chem Intermed (2013) 39:185–204
DOI 10.1007/s11164-012-0642-6

Photoinduced charge separation of phenothiazine–platinum–naphthalene diimide triads linked by twisted phenylene bridges

Ryoji Sugimura · Shuichi Suzuki · Masatoshi Kozaki · Kazutoshi Keyaki · Koichi Nozaki · Hironori Matsushita · Noriaki Ikeda · Keiji Okada

Received: 3 October 2011 / Accepted: 5 December 2011 / Published online: 10 July 2012

Abstract Two triads (i.e., 3PTZ–Pt–MNDI and 10PTZ–Pt–MNDI) consisting of 3-phenothiazine (3PTZ) or 10-phenothiazine (10PTZ), bipyridine–diacetylide platinum complex (Pt), and naphthalene diimide (MNDI) chromophores linked by highly twisted biphenylene spacers have been prepared. The formation and decay of the charge-separated (CS) states in toluene were studied by use of picosecond and nanosecond laser photolysis via selective excitation of the Pt moiety. The time required for formation of the CS state, PTZ^{+}–Pt–$MNDI^{-}$, from PTZ–$^{3}Pt^{*}$–MNDI was determined to be $\tau_{CS} = 280$ ps for $3PTZ^{+}$–Pt–$MNDI^{-}$ and $\tau_{CS} = 230$ ps for $10PTZ^{+}$–Pt–$MNDI^{-}$. The lifetimes of the CS states were determined to be $\tau_{CR1} = 75$ ns (95 %) and $\tau_{CR2} = 285$ ns (5 %) for $3PTZ^{+}$–Pt–$MNDI^{-}$ and $\tau_{CR} = 830$ ns for $10PTZ^{+}$–Pt–$MNDI^{-}$. Formation and decay of the CS states are discussed in terms the Marcus theory and the spin-correlated radical pair mechanism.

R. Sugimura · S. Suzuki · M. Kozaki · K. Okada (✉)
Department of Chemistry, Graduate School of Science, Osaka City University, Sumiyoshi-ku, Osaka 558-8585, Japan
e-mail: okadak@sci.osaka-cu.ac.jp

K. Keyaki · K. Nozaki (✉)
Department of Chemistry, Graduate School of Science and Engineering, University of Toyama, Gofuku, Toyama 930-8555, Japan
e-mail: nozaki@sci.u-toyama.ac.jp

H. Matsushita · N. Ikeda (✉)
Department of Macromolecular Science and Engineering, Graduate School of Science and Technology, Kyoto Institute of Technology, Sakyo-ku, Kyoto 606-8585, Japan
e-mail: ikeda@kit.ac.jp

Keywords Photoinduced electron transfer · Phenothiazine · Naphthalene diimide · Platinum complex

Introduction

Photoinduced charge separation is a fundamental and crucial process for energy conversion from light to storable electric or chemical energy. In bacteria, a natural photosynthetic system enables very fast (within 150 fs) energy transfer to a special pair (i.e., SP: $Bchl_2$). Electron transfer to bacteriopheophytin in the L unit (BPh_L) then results in the formation of a charge-separated (CS) state, $Bchl_2^+BPhL^-$, in 3 ps and ubiquinone Q_A in 200 ps to efficiently yield $Bchl_2^+Q_A^-$. In this CS state, the charges are separated by 35 Å in the protein matrix. $Bchl_2^+Q_A^-$ has a long lifetime of 100 ms in the absence of Q_B [1]. To date, a number of artificial systems featuring multi-chromophoric donor–acceptors have been designed and synthesized to obtain long-lived CS states [2]. However, these systems do not always produce long-lived CS states. One promising strategy for obtaining long-lived CS states is the spin-control approach [3], which uses a chromophore with ultrafast intersystem crossing. Metal complexes containing Ru, Ir, and Pt emit intense phosphorescence at room temperature because of strong spin–orbit coupling (SOC) and are expected to be good sensitizers for generation of triplet CS states [4–11]. These triplet CS states recombine slowly to the singlet ground states because of the spin-forbidden nature of the transformation. We recently reported that MTA–Pt–MNDI (**1**), which features a bipyridine–diacetylide platinum complex (Pt) linked with a dimethoxydimethyl-triphenylamine (MTA) moiety as the donor and a naphthalene diimide (MNDI) moiety as the acceptor, produced a long-lived CS state with high efficiency ($\tau_{CS} \approx 1$ μs, $\Phi_{CS} = 0.96$) [12]. In this complex, MTA and MNDI are bound to the Pt atom through highly twisted phenylene linkers which enable rapid electron (hole) shift (MTA^+–Pt^-–MNDI (or MTA–Pt^+–$MNDI^-$) → MTA^+–Pt–$MNDI^-$) but reduce back-electron transfer (i.e., MTA^+–Pt^-–MNDI (or MTA–Pt^+–$MNDI^-$) → MTA–Pt–MNDI) in the initially formed geminate ion pair. As a result, the long-separated final ion pair MTA^+–Pt–$MNDI^-$ is efficiently produced. The final CS state was shown to be a spin-correlated radical pair (SCRP) state [12] with a precursor MTA–^{3}Pt*–MNDI state that is generated by the SOC-induced ultrafast intersystem crossing (ISC) of MTA–^{1}Pt*–MNDI. In this study, we apply this methodology to phenothiazine (PTZ)-based triads; i.e., 3-phenothiazine (3PTZ)–Pt–MNDI (**2**) and 10-phenothiazine (10PTZ)–Pt–MNDI (**3**). Compounds **2** (E^{ox1}: +0.21 V vs. Fc^+/Fc in CH_2Cl_2) and **3** (E^{ox1}: +0.25 V) have similar oxidation potentials to **1** (E^{ox1}: +0.16 V), suggesting they undergo similar photoinduced electron-transfer reactions. Compounds **2** and **3** are positional isomers and have very similar oxidation potentials, because of the common PTZ moieties and similar distances between PTZ and MNDI. Hence, the forces driving charge recombination in the CS states in these positional isomers are similar. However, the rates of charge recombination (CR) to the respective ground states were found to be very different. This paper describes the details of the CS and CR processes for the photoexcitation of **2** and **3** using the picosecond and nanosecond transient absorption method.

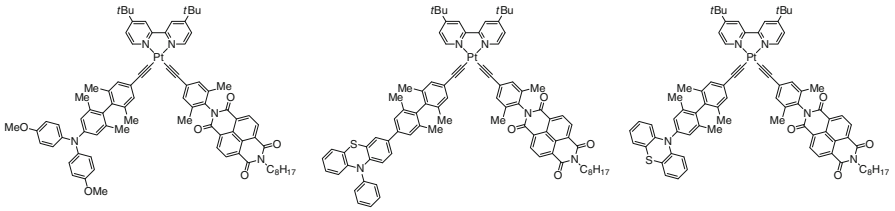

MTA-Pt-MNDI (1) 3PTZ-Pt-MNDI (2) 10PTZ-Pt-MNDI (3)

Experimental

General procedure

^{1}H NMR spectra were recorded with a Jeol JNM-LA400 spectrometer. FAB-MS and HRMS spectra were recorded with Jeol JMS-AX-500 and JMS-AX-700 spectrometers, respectively. Infrared spectra were recorded on KBr plates with a Shimadzu FTIR-8700 spectrometer. Melting points were measured with a hot-stage apparatus and are uncorrected. Absorption and luminescence spectra were measured with a Jasco V-750 UV–visible spectrometer and a Shimadzu RF-5300 PC fluorophotometer. Silica gel 60 (100–200 mesh) and aluminium oxide 90 (70–230 mesh) were used for column chromatography. All commercially available compounds were reagent grade and used without further purification. Toluene and THF were dried and distilled over sodium. CH_2Cl_2, diisopropylamine (iPr$_2$NH), *N*-ethyldiisopropylamine (iPr$_2$NEt), and *o*-dichlorobenzene were dried and distilled over calcium hydride. 3-Amino-10-phenyl-10*H*-phenothiazine (**4**) [13], 4,4′-diiodo-2,2′,6,6′-tetramethylbiphenyl (**8**) [12, 14], *N*-(4-ethynyl-2,6-dimethylphenyl)-*N*′-(*n*-octyl) naphthalene-1,8:4,5-tetracarboxydiimide (**12**) [12], 4,4′-di-*tert*-butyl-2,2′-bipyridine platinum dichloride (**13**) [15], and *N*-(4-bromo-2,6-dimethylphenyl)-*N*′-(*n*-octyl)naphthalene-1,8:4,5-tetracarboxydiimide (**23**) [12] were prepared by methods described in the literature. The 10-(4′-*tert*-butylphenyl)-10*H*-phenothiazine (**22**) was prepared from phenothiazine (**16**) and 1-bromo-4-*tert*-butylbenzene by the cross coupling reaction using $Pd_2(dba)_3$-*t*BuOK in toluene.

*Synthesis of 3-[(1E)-3,3-diethyltriaz-1-en-1-yl]-10-phenyl-10H-phenothiazine (**5**)*

3-Amino-10-phenyl-10*H*-phenothiazine (**4**) (1.12 g, 3.86 mmol) and CH_2Cl_2 (20 mL) were placed in a 50-mL two-necked flask. The solution was cooled to 0 °C in an ice bath. $BF_3{\cdot}OEt_2$ (0.98 mL, 7.72 mmol) was added to the flask and the mixture was stirred for 40 min under nitrogen. A solution of *tert*-butyl nitrite (0.69 mL, 5.79 mmol) in CH_2Cl_2 (3 mL) was slowly added to the flask, and the mixture was stirred for 1 h. K_2CO_3 (2.67 g, 19.3 mmol) and Et_2NH (2.4 mL) were added to the flask, and the mixture was stirred at room temperature for 20 h. The mixture was filtered to remove insoluble materials which were washed with a small amount of CH_2Cl_2. The filtrate was poured into water. The organic layer was separated, and washed with water, dried over Na_2SO_4, filtered, and concentrated under reduced pressure. The resulting mixture was separated and purified by

alumina column chromatography using hexane–CH_2Cl_2 (2:1 v/v) as eluent, to give triazene **5** (1.28 g, 89 %) as an orange solid. **5**: $C_{22}H_{22}N_4S$; MW 374.50; mp: 100–102 °C; ^{1}H NMR (400 MHz, DMSO-d_6) δ (ppm): 7.66 (*t*, $J = 7.3$ Hz, 2H), 7.52 (*t*, $J = 7.3$ Hz, 1H), 7.40 (d, $J = 7.1$ Hz, 2H), 7.08 (dd, $J = 7.6$, 1.4 Hz, 1H), 7.05 (d, $J = 2.2$ Hz, 1H), 6.96–6.84 (m, 3H), 6.16 (*t*, $J = 8.8$ Hz, 2H), 3.68 (m, 4H), 1.16 (s (br), 6H); IR (KBr/cm^{-1}) 2974, 1589, 1495, 1462, 1391, 1352, 1304, 1236, 1192, 1105, 893, 812, 772, 743, 698, 638, 544; MS (FAB$^+$) = 374.19 [M$^+$]. High-resolution MS: found *m/z* 374.1567; calcd for $C_{22}H_{22}N_4S$ *m/z* 374.1565.

*Synthesis of 3-iodo-10-phenyl-10H-phenothiazine (**6**)*

Triazene **5** (1.63 g, 4.35 mmol) was placed in a screw-capped tube. The tube was flushed with nitrogen. CH_3I (8 mL) and I_2 (2.21 g, 8.70 mmol) were added, and the tube was sealed and heated at 55 °C for 2 h. CH_2Cl_2 was added, and the mixture and washed with aqueous $NaHSO_3$ and water. The organic layer was dried over Na_2SO_4, filtered, and concentrated under reduced pressure. The mixture was separated and purified by alumina column chromatography using hexane–CH_2Cl_2 (5:1 v/v) as eluent, to give **6** (1.33 g, 76 %) as a pale yellow solid. **6**: $C_{18}H_{12}INS$; MW 401.26; mp: 107–109 °C; ^{1}H NMR (400 MHz, DMSO-d_6) δ (ppm): 7.68 (*t*, $J = 7.3$ Hz, 2H), 7.56 (*t*, $J = 7.6$ Hz, 1H), 7.42 (d, $J = 7.3$ Hz, 2H), 7.38 (d, $J = 2.2$ Hz, 1H), 7.23 (dd, $J = 8.6$, 2.2 Hz, 1H), 7.07 (dd, $J = 7.3$, 1.7 Hz, 1H), 6.93 (d*t*, $J = 7.6$, 1.7 Hz, 1H), 6.86 (d*t*, $J = 7.6$, 1.2 Hz, 1H), 6.10 (dd, $J = 7.8$, 1.2 Hz, 1H), 5.89 (d, $J = 8.6$ Hz, 1H); IR (KBr/cm^{-1}) 1583, 1558, 1491, 1456, 1439, 1377, 1302, 1258, 1240, 1130, 1069, 1042, 870, 851, 808, 781, 746, 696, 629, 538. High-resolution MS: found *m/z* 400.9730; calcd for $C_{18}H_{12}INS$ *m/z* 400.9735.

*Synthesis of 10-phenyl-3-(4,4,5,5-tetramethyl-1,3,2-dioxaborolan-2-yl)-10H-phenothiazine (**7**)*

Compound **6** (1.25 g, 3.12 mmol), bis(pinacolato)diboron (1.19 g, 4.67 mmol), [1,1′-bis(diphenylphosphino)ferrocene]dichloropalladium(II) (255 mg, 0.312 mmol), and KOAc (919 mg, 9.36 mmol) were dissolved in DMSO (20 mL) in a two-necked flask. The mixture was stirred at 80 °C for 1 h under nitrogen. After cooling to room temperature, the mixture was filtered through a Celite pad. The Celite pad was washed with EtOAc. The combined filtrate was washed with water (ca 100 mL), dried over Na_2SO_4, and concentrated under reduced pressure. The resulting mixture was separated and purified by silica gel column chromatography using hexane–CH_2Cl_2 (2:1 v/v) as eluent, to give **7** (997 mg, 80 %) as a pale yellow solid. **7**: $C_{24}H_{24}BNO_2S$; MW 401.33; mp: 156–158 °C; ^{1}H NMR (400 MHz, DMSO-d_6) δ (ppm): 7.70 (*t*, $J = 7.3$ Hz, 2H), 7.57 (*t*, $J = 7.6$ Hz, 1H), 7.42 (d, $J = 7.3$ Hz, 2H), 7.23 (d, $J = 1.5$ Hz, 1H), 7.18 (dd, $J = 8.0$, 1.5 Hz, 1H), 7.05 (dd, $J = 7.3$, 1.7 Hz, 1H), 6.91 (d*t*, $J = 7.6$, 1.7 Hz, 1H), 6.85 (d*t*, $J = 7.6$, 1.2 Hz, 1H), 6.09 (d, $J = 8.0$ Hz, 1H), 6.07 (dd, $J = 7.8$, 1.2 Hz, 1H), 1.25 (s, 12H); IR (KBr/cm^{-1}) 2980, 2932, 1603, 1589, 1576, 1491, 1470, 1441, 1404, 1383, 1354, 1302, 1258, 1144, 1105, 962, 866, 824, 775, 750, 698, 667, 629, 536; MS (FAB$^+$) = 401.20 [M$^+$]. High-resolution MS: found *m/z* 401.1616; calcd for $C_{24}H_{24}BNO_2S$ *m/z* 401.1621.

*Synthesis of 3-(4′-iodo-2,2′,6,6′-tetramethylbiphenyl-4-yl)-10-phenyl-10H-phenothiazine (**9**)*

Compound **7** (450 mg, 1.12 mmol), 4,4′-diiodo-2,2′,6,6′-tetramethylbiphenyl (**8**) (1.55 g, 3.36 mmol), Cs_2CO_3 (730 mg, 2.24 mmol), and $Pd(OAc)_2$ (12.6 mg, 0.056 mmol) were dissolved in DMF (20 mL) in a two-necked flask. The solution was stirred at 110 °C for 1 h under nitrogen. After cooling to room temperature, the mixture was filtered through a Celite pad. The Celite pad was washed with CH_2Cl_2. The combined filtrate was concentrated under reduced pressure. The resulting residue was separated and purified by alumina column chromatography using hexane–CH_2Cl_2 (6:1 v/v) as eluent, to give **9** (516 mg, 76 %) as a pale yellow solid. **9**: $C_{34}H_{28}INS$; MW 609.56; mp: 219–221 °C; ^{1}H NMR (400 MHz, DMSO-d_6) δ (ppm): 7.70 (*t*, $J = 7.3$ Hz, 2H), 7.58 (*t*, $J = 7.6$ Hz, 1H), 7.56 (s, 2H), 7.47 (d, $J = 7.3$ Hz, 2H), 7.43 (d, $J = 2.2$ Hz, 1H), 7.39 (s, 2H), 7.28 (dd, $J = 8.6$, 2.2 Hz, 1H), 7.10 (dd, $J = 7.3$, 1.5 Hz, 1H), 6.94 (d*t*, $J = 7.6$, 1.5 Hz, 1H), 6.87 (d*t*, $J = 7.6$, 1.2 Hz, 1H), 6.19 (d, $J = 8.6$ Hz, 1H), 6.14 (dd, $J = 7.3$, 1.2 Hz, 1H), 1.86 (s, 6H), 1.81 (s, 6H); IR (KBr/cm^{-1}) 1576, 1493, 1466, 1439, 1377, 1312, 1259, 999, 866, 816, 745, 698, 540; MS (FAB$^+$) = 609.22 [M$^+$]. High-resolution MS: found *m*/*z* 609.0989; calcd for $C_{34}H_{28}INS$ *m*/*z* 609.0987.

*Synthesis of 10-phenyl-3-{2,2′,6,6′-tetramethyl-4′-[(trimethylsilyl)ethynyl]biphenyl-4-yl}-10H-phenothiazine (**10**)*

Compound **9** (450 mg, 0.738 mmol), $PdCl_2(PPh_3)_2$ (51.8 mg, 0.0738 mmol), CuI (14.1 mg, 0.0738 mmol), THF (5 mL), and iPr$_2$NEt (2.5 mL) were placed in a screw-capped tube. The tube was flushed with nitrogen. Trimethysilylacetylene (0.125 mL, 0.886 mmol) was added. The tube containing the mixture was sealed and heated at 70 °C for 6 h. The solvents were evaporated under reduced pressure. The residue was separated and purified by silica gel column chromatography using hexane–CH_2Cl_2 (6:1 v/v) as eluent, to give **10** (380 mg, 89 %) as a pale yellow solid. **10**: $C_{39}H_{37}NSSi$; MW 579.87; pale yellow solid; mp: 209–211 °C; ^{1}H NMR (400 MHz, DMSO-d_6) δ (ppm): 7.71 (*t*, $J = 8.1$ Hz, 2H), 7.58 (*t*, $J = 7.3$ Hz, 1H), 7.47 (d, $J = 7.3$ Hz, 2H), 7.43 (d, $J = 2.2$ Hz, 1H), 7.40 (s, 2H), 7.29 (s, 2H), 7.29–7.27 (m, 1H), 7.10 (dd, $J = 7.3$, 1.2 Hz, 1H), 6.94 (d*t*, $J = 7.6$, 1.2 Hz, 1H), 6.87 (d*t*, $J = 7.3$, 1.2 Hz, 1H), 6.19 (d, $J = 8.8$ Hz, 1H), 6.14 (dd, $J = 8.1$, 1.2 Hz, 1H), 1.85 (s, 6H), 1.83 (s, 6H), 0.24 (s, 9H); IR (KBr/cm^{-1}) 2957, 2918, 2152, 1593, 1578, 1493, 1464, 1439, 1377, 1310, 1250, 1160, 1020, 1001, 854, 748, 698, 648, 540; MS (FAB$^+$) = 579.36 [M$^+$]. High-resolution MS: found *m*/*z* 579.2407; calcd for $C_{39}H_{37}NSSi$ *m*/*z* 579.2416.

*Synthesis of 2-(4′-ethynyl-2,2′,6,6′-tetramethylbiphenyl-4-yl)-10-phenyl-10H-phenothiazine (**11**)*

Compound **10** (292 mg, 0.504 mmol) was dissolved in THF (15 mL). To this solution, 1.0 M THF solution of $Bu_4N^+{\cdot}F^-$ (0.63 mL, 0.63 mmol) was added and the mixture was stirred at room temperature for 15 min. CH_2Cl_2 (ca 50 mL) was

added to the mixture and washed with water. The organic layer was separated, dried over Na_2SO_4, filtered, and concentrated. The mixture was separated by alumina column chromatography using hexane–CH_2Cl_2 (6:1 v/v) as eluent, to give **11** (251 mg, 98 %) as a yellow powder. **11**: $C_{36}H_{29}NS$; MW 507.69; yellow solid; mp: 229–231 °C; ^{1}H NMR (400 MHz, DMSO-d_6) δ (ppm): 7.71 (*t*, $J = 8.0$ Hz, 2H), 7.58 (*t*, $J = 7.3$ Hz, 1H), 7.47 (d, $J = 7.3$ Hz, 2H), 7.43 (d, $J = 2.2$ Hz, 1H), 7.40 (s, 2H), 7.29 (s, 2H), 7.29–7.27 (m, 1H), 7.10 (dd, $J = 7.3$, 1.2 Hz, 1H), 6.94 (d*t*, $J = 7.4$, 1.2 Hz, 1H), 6.87 (d*t*, $J = 7.4$, 1.2 Hz, 1H), 6.19 (d, $J = 8.3$ Hz, 1H), 6.14 (d, $J = 8.0$ Hz, 1H), 4.11 (s, 1H), 1.86 (s, 6H), 1.84 (s, 6H); IR (KBr/cm^{-1}) 3292, 2914, 1593, 1576, 1491, 1466, 1439, 1377, 1312, 1265, 1244, 1001, 866, 816, 775, 743, 710, 698, 650, 613, 540. High-resolution MS: found *m/z* 507.2021; calcd for $C_{36}H_{29}NS$ *m/z* 507.2021.

*Synthesis of 3PTZ–Pt–MNDI (**2**)*

Compound **11** (100 mg, 0.197 mmol), **12** (100 mg, 0.197 mmol), **13** (105 mg, 0.197 mmol), and CuI (3.8 mg, 0.020 mmol) were placed in a two-necked flask. CH_2Cl_2 (14 mL) and *i*Pr_2NH (0.7 mL) were added and the flask was flushed with nitrogen. The mixture was stirred at room temperature for 18 h. The solvents were evaporated under reduced pressure. The resulting mixture was separated and purified by alumina column chromatography to give **14** (58.2 mg, 20 %, eluent: hexane–CH_2Cl_2 1:1 v/v), **2** (99.7 mg, 34 %, eluent: CH_2Cl_2), and **15** (58.9 mg, 20 %, eluent: CH_2Cl_2–EtOAc 10:1 v/v). Analytically pure samples were obtained by reprecipitation from CH_2Cl_2 with ether. **14**: $C_{90}H_{80}N_4PtS_2$; MW 1476.84; brown solid; mp: >300 °C; ^{1}H NMR (400 MHz, $CDCl_3$) δ (ppm): 9.81 (d, $J = 6.1$ Hz, 2H), 7.95 (d, $J = 2.0$ Hz, 2H), 7.65–7.59 (m, 6H), 7.50 (*t*, $J = 7.6$ Hz, 2H), 7.43 (dd, $J = 8.3$, 1.5 Hz, 4H), 7.34 (s, 4H), 7.32 (d, $J = 2.2$ Hz, 2H), 7.22 (s, 4H), 7.11 (dd, $J = 8.5$, 2.2 Hz, 2H), 7.04 (dd, $J = 7.1$, 1.7 Hz, 2H), 6.87–6.79 (m, 4H), 6.23 (d, $J = 8.5$ Hz, 2H), 6.19 (dd, $J = 8.0$, 1.4 Hz, 2H), 1.94 (s, 12H), 1.87 (s, 12H), 1.45 (s, 18H); IR (KBr/cm^{-1}) 3061, 2965, 2916, 2870, 2100, 1593, 1547, 1493, 1464, 1441, 1418, 1375, 1308, 1252, 1204, 1155, 1130, 1074, 1001, 866, 814, 775, 745, 698, 600, 542, 419. High-resolution MS: found *m/z* 1475.5458; calcd for $C_{90}H_{80}N_4PtS_2$ *m/z* 1475.5472. 3PTZ–Pt–MNDI (**2**): $C_{86}H_{81}N_5O_4PtS$; MW 1475.74; brown solid; mp: ca 274 °C (dec); ^{1}H NMR (400 MHz, $CDCl_3$) δ (ppm): 9.80 (d, $J = 6.1$ Hz, 1H), 9.74 (d, $J = 6.1$ Hz, 1H), 8.83 (d, $J = 7.6$ Hz, 2H), 8.80 (d, $J = 7.6$ Hz, 2H), 7.95 (d, $J = 2.0$ Hz, 2H), 7.65–7.61 (m, 4H), 7.50 (*t*, $J = 7.6$ Hz, 1H), 7.44–7.42 (m, 4H), 7.34 (s, 2H), 7.32 (d, $J = 2.0$ Hz, 1H), 7.23 (s, 2H), 7.12 (dd, $J = 8.6$, 2.2 Hz, 1H), 7.04 (dd, $J = 7.1$, 2.0 Hz, 1H), 6.87–6.79 (m, 2H), 6.23 (d, $J = 8.6$ Hz, 1H), 6.19 (dd, $J = 8.0$, 1.2 Hz, 1H), 4.22 (*t*, $J = 7.6$ Hz, 2H), 2.09 (s, 6H), 1.94 (s, 6H), 1.88 (s, 6H), 1.74 (m, 2H), 1.46–1.28 (m, 28H), 0.88 (*t*, $J = 6.4$ Hz, 3H); IR (KBr/cm^{-1}) 2959, 2924, 2856, 2104, 1709, 1670, 1618, 1580, 1547, 1464, 1418, 1369, 1339, 1308, 1248, 1192, 1155, 1130, 1076, 1024, 1001, 976, 868, 849, 824, 793, 770, 745, 700, 602, 419. High-resolution MS: found *m/z* 1474.5665; calcd for $C_{86}H_{81}N_5O_4PtS$ *m/z* 1474.5657.

*Synthesis of 10-(4′-iodo-2,2′,6,6′-tetramethylbiphenyl-4-yl)-10H-phenothiazine (**17**)*

Phenothiazine (**16**) (200 mg, 1.00 mmol), 4,4′-diiodo-1,1′,3,3′-tetramthylbiphenyl (**8**) (1.39 g, 3.01 mmol), copper powder (127 mg, 2.00 mmol), K_2CO_3 (553 mg, 4.00 mmol), and 18-crown-6-ether (26 mg, 0.098 mmol) were placed in a 50-mL two-necked flask. *o*-Dichlorobenzene (5 mL) was added to the flask and the mixture was heated under reflux for 4 h under nitrogen. After cooling to room temperature, the mixture was filtered through a Celite pad. The Celite pad was washed with CH_2Cl_2 ($\sim$30 mL). The filtrate was concentrated under reduced pressure. The residue was separated and purified by silica gel column chromatography using hexane–CH_2Cl_2 (10:1 v/v) as eluent to give compound **17** (344 mg, 64 %) as a pale yellow solid. **17**: $C_{28}H_{24}INS$; MW 533.47; mp: 220–222 °C; ^{1}H NMR (400 MHz, DMSO-d_6) δ (ppm): 7.62 (s, 2H), 7.24 (s, 2H), 7.07 (dd, $J = 7.4$, 1.6 Hz, 2H), 6.98 (d*t*, $J = 8.2$, 1.6 Hz, 2H), 6.86 (d*t*, $J = 7.4$, 1.2 Hz, 2H), 6.27 (dd, $J = 8.2$, 1.2 Hz, 2H), 1.91 (s, 12H); IR (KBr/cm^{-1}); 1589, 1574, 1489, 1464, 1443, 1377, 1310, 1246, 1232, 1128, 1047, 1001, 856, 827, 800, 741, 652. High-resolution MS: found *m*/*z* 533.0673; calcd for $C_{28}H_{24}INS$ *m*/*z* 533.0674.

*Synthesis of 10-{2,2′,6,6′-tetramethyl-4′-[(trimethylsilyl)ethynyl]biphenyl-4-yl}-10H-phenothiazine (**18**)*

Compound **17** (150 mg, 0.281 mmol), $PdCl_2(PPh_3)_2$ (20 mg, 0.028 mmol), CuI (5.4 mg, 0.028 mmol), THF (4 mL), and iPr_2NEt (2 mL) were placed in a screw-capped tube. The tube was flushed with nitrogen. Trimethysilylacetylene (0.048 mL, 0.337 mmol) was added, and the tube was sealed and heated at 80 °C for 3 h. The solvent was evaporated under reduced pressure. The residue was separated and purified by silica gel column chromatography using hexane–CH_2Cl_2 (6:1 v/v) as eluent, to give **18** (142 mg, quant) as a pale yellow solid. **18**: $C_{33}H_{33}NSSi$; MW 503.77; mp: 187–189 °C; ^{1}H NMR (400 MHz, DMSO-d_6) δ (ppm): 7.33 (s, 2H), 7.24 (s, 2H), 7.08 (dd, $J = 7.4$, 1.5 Hz, 2H), 6.99 (d*t*, $J = 7.4$, 1.6 Hz, 2H), 6.86 (d*t*, $J = 7.4$, 1.2 Hz, 2H), 6.29 (dd, $J = 8.2$, 1.1 Hz, 2H), 1.93 (s, 6H), 1.90 (s, 6H), 0.25 (s, 9H); IR (KBr/cm^{-1}); 2957, 2920, 2152, 1589, 1572, 1485, 1462, 1443, 1379, 1308, 1248, 1238, 1163, 1128, 1043, 1020, 1003, 928, 843, 745, 708, 654. High-resolution MS: found *m*/*z* 503.2104; calcd for $C_{33}H_{33}NSSi$ *m*/*z* 503.2103.

*Synthesis of 10-(4′-ethynyl-2,2′,6,6′-tetramethylbiphenyl-4-yl)-10H-phenothiazine (**19**)*

Compound **18** (100 mg, 0.119 mmol) was dissolved in THF (6 mL). To the solution, 1.0 M THF solution of $Bu_4N^+{\cdot}F^-$ (0.25 mL, 0.25 mmol) was added and the mixture was stirred at room temperature for 1 h. CH_2Cl_2 (ca 30 mL) was added to the mixture and washed with water. The organic layer was separated, dried over Na_2SO_4, filtered, and concentrated. The mixture was separated by alumina column chromatography using hexane–CH_2Cl_2 (5:1 v/v) as eluent, to give **19** (74 mg, 86 %) as a pale yellow powder. **19**: $C_{30}H_{25}NS$; MW 431.59; mp: 224–226 °C; ^{1}H NMR

(400 MHz, DMSO-d_6) δ (ppm): 7.35 (s, 2H), 7.24 (s, 2H), 7.07 (dd, $J = 7.4$, 1.5 Hz, 2H), 6.99 (d*t*, $J = 8.2$, 1.5 Hz, 2H), 6.86 (d*t*, $J = 7.4$, 1.2 Hz, 2H), 6.28 (dd, $J = 8.2$, 1.2 Hz, 2H), 4.15 (s, 1H), 1.94 (s, 6H), 1.91 (s, 6H); IR (KBr/cm^{-1}); 3312, 2916, 1591, 1576, 1489, 1464, 1441, 1375, 1308, 1279, 1246, 1234, 1049, 1003, 876, 741, 638, 606, 419. High-resolution MS: found *m/z* 431.1727; calcd for $C_{30}H_{25}NS$ *m/z* 431.1708.

*Synthesis of 10PTZ–Pt–MNDI (**3**)*

Compound **19** (100 mg, 0.232 mmol), **12** (117 mg, 0.232 mmol), **13** (124 mg, 0.232 mmol), and CuI (5.3 mg, 0.028 mmol) were placed in a two-necked flask. CH_2Cl_2 (15 mL) and *i*Pr_2NH (0.75 mL) were added and the flask was flushed with nitrogen. The mixture was stirred at room temperature for 18 h. The solvents were evaporated under reduced pressure. The resulting mixture was separated and purified by alumina column chromatography to give **20** (65.7 mg, 21 %, eluent: hexane–CH_2Cl_2 1:2 v/v), **3** (117 mg, 36 %, eluent: CH_2Cl_2), and **15** (75.2 mg, 22 %, eluent: CH_2Cl_2–EtOAc 10:1 v/v). Analytically pure samples were obtained by reprecipitation from CH_2Cl_2 with ether. **20**: $C_{78}H_{72}N_4PtS_2$; MW 1324.65; brown solid; mp: >300 °C; ^{1}H NMR (400 MHz, $CDCl_3$) δ (ppm): 9.82 (d, $J = 5.8$ Hz, 2H), 7.97 (d, $J = 1.4$ Hz, 2H), 7.63 (dd, $J = 5.8$, 2.0 Hz, 2H), 7.40 (s, 4H), 7.14 (s, 4H), 7.00 (dd, $J = 7.3$, 1.4 Hz, 4H), 6.89 (d*t*, $J = 8.2$, 1.4 Hz, 4H), 6.80 (d*t*, $J = 7.3$, 1.2 Hz, 4H), 6.31 (dd, $J = 8.2$, 1.2 Hz, 4H), 1.99 (s, 12H), 1.96 (s, 12H), 1.47 (s, 18H); IR (KBr/cm^{-1}) 3404, 2964, 2914, 2106, 1618, 1589, 1547, 1462, 1443, 1418, 1377, 1308, 1236, 1159, 1126, 1086, 1042, 1001, 928, 870, 847, 745, 654, 600, 563; MS (FAB$^+$) = 1325 [M$^+$]. Anal. Calcd for $C_{78}H_{72}N_4PtS_2$: C, 70.72; H, 5.48; N, 4.23. Found: C, 70.37; H, 5.43; N, 3.97. 10PTZ–Pt–MNDI (**3**): $C_{80}H_{77}N_5O_4PtS$; MW 1399.65; brown solid; mp: 268 °C (dec); ^{1}H NMR (400 MHz, $CDCl_3$) δ (ppm): 9.81 (d, $J = 6.1$ Hz, 1H), 9.75 (d, $J = 6.1$ Hz, 1H), 8.83 (d, $J = 7.6$ Hz, 2H), 8.80 (d, $J = 7.6$ Hz, 2H), 7.97 (s, 2H), 7.63 (d*t*, $J = 6.1$, 2.0 Hz, 2H), 7.43 (s, 2H), 7.40 (s, 2H), 7.14 (s, 2H), 7.00 (dd, $J = 7.6$, 1.6 Hz, 2H), 6.89 (d*t*, $J = 7.6$, 1.7 Hz, 2H), 6.80 (d*t*, $J = 7.3$, 1.2 Hz, 2H), 6.31 (dd, $J = 8.3$, 1.2 Hz, 2H), 4.23 (*t*, $J = 7.6$ Hz, 2H), 2.10 (s, 6H), 1.99 (s, 6H), 1.96 (s, 6H), 1.76 (m, 2H), 1.47–1.26 (m, 28H), 0.88 (*t*, $J = 6.8$ Hz, 3H); IR (KBr/cm^{-1}) 2959, 2924, 2856, 2106, 1709, 1670, 1618, 1582, 1545, 1462, 1445, 1418, 1369, 1340, 1308, 1248, 1192, 1045, 872, 824, 793, 770, 745, 706, 419. High-resolution MS: found *m/z* 1398.5342; calcd for $C_{80}H_{77}N_5O_4PtS$ *m/z* 1398.5344.

Measurement of cyclic voltammograms

Redox potentials were measured, by use of an ALS model 610A electrochemical analyzer, in a conventional three-electrode cell equipped with a glassy carbon working electrode, a platinum wire counter electrode, and a saturated calomel electrode (SCE) as reference electrode. Measurements were performed with a sweep rate of 100 mV/s in a suitable solvent containing 0.1 M tetra-*n*-butylammonium perchlorate as supporting electrolyte. The redox potentials were finally corrected on the basis of the ferrocene/ferrocenium (Fc/Fc$^+$) couple.

Measurements of absorption spectra for phenothiazine radical cation $\mathbf{9}^+$ and $\mathbf{22}^+$, and naphthalene diimide radical anion $\mathbf{23}^-$

For assignment of transient species in laser photolysis, the absorption spectra of the electrochemically generated $\mathbf{9}^+$, $\mathbf{22}^+$, and $\mathbf{23}^-$ were measured by use of an Ocean Optics HR4000 spectrometer with a 1 mm width electrochemical cell equipped with a fine platinum mesh working electrode, a platinum wire as a counter electrode, and a reference SCE ($Fc/Fc^+ = +0.48$ V vs. SCE in CH_2Cl_2 and DMF) at suitable external potentials. The radical cation and radical anion species were generated in CH_2Cl_2 and in DMF, respectively, in the presence of 0.1 M tetra-*n*-butylammonium perchlorate.

Molecular geometry and molecular orbital calculations for model compounds **2M** and **3M**

Model compounds **2M** and **3M**, in which, for simplicity methyl groups were used instead of the *tert*-butyl groups on bipyridine and the *n*-octyl group on MNDI in **2** and **3**, were used for geometrical optimization and molecular orbital calculations for **2** and **3**. There are two relative orientations (parallel and perpendicular toward the standard Pt-plane) of the phenyl rings, A and B (formula **24**), thus four basic structures of conformers in PTZ-Pt-MNDI (**2M** and **3M**) can be derived. More conformers are generated from these basic conformers depending on the folding direction and orientations of PTZs: 10-Phenylphenothiazine has a largely twisted (almost perpendicular) phenyl ring in the 10-position. In 10PTZ–Pt–MNDI (**3M**), there are two folding directions in the PTZ rings of the perpendicular orientation. Therefore, 10PTZ–Pt–MNDI (**3M**) has two more conformers, six (4 + 2) conformers in total. In 3PTZ-Pt-MNDI (**2M**), there are eight conformers (two folding directions and four possible rotational orientations) for each basic conformer. Therefore, 3PTZ–Pt–MNDI (**2M**) has 32 (4 × 8) conformers in total. The initial geometry of these conformers was generated. Geometrical optimization was performed using MOPAC 2009 (PM6) [16]. The energies of thus obtained conformers are as follows: 180.63019–181.25674 kcal/mol for 3PTZ–Pt–MNDI (**2M**) and 156.67625–157.32413 kcal/mol for 10PTZ–Pt–MNDI (**3M**). The most stable conformational isomers and their HOMO and LUMO are depicted in Fig. 2.

Laser photolysis of **2** and **3**

Nanosecond time-resolved difference spectra were obtained by using the second harmonic generator of a Q-switched Nd^{3+}:YAG laser (Continuum Surelite I-10, $\lambda = 532$ nm) [17]. Sample solutions in a 1 cm-quartz cell were deaerated by bubbling with argon for 5 min. White light from a Xe-arc lamp was used for acquisition of absorption spectra. For measurements of picosecond time-resolved difference spectra, a sample solution in a quartz cell (1 mm length) was excited with the second harmonic pulses of a mode-locked Nd^{3+}:YAG laser (Continuum PY61C-10, $\lambda = 532$ nm) [18]. The transient absorption spectra in the time range −20 ps to 1 ns were acquired by using continuum pulses generated by focusing the fundamental laser pulse into a flowing H_2O/D_2O mixture (1:1 by volume).

Results and discussion

Synthesis of PTZ–Pt–MNDIs (**2** and **3**)

The synthesis of **2** is outlined in Scheme 1. Compound **4** was converted to triazene derivative **5** followed by treatment with CH_3I and I_2 to give 3-iodophenothiazine **6**. Compound **6** was reacted with bis(pinacolato)diboron in the presence of Pd as catalyst to give borate **7**. The Pd-mediated cross-coupling of **7** with diiodobiphenyl **8** produced **9** in moderate yield. Then, acetylene derivative **11** was obtained from **9** via **10**. Triad **2** was prepared by reaction of bipyridine–platinum–dichloride complex **13** with an equimolar mixture of **11** and **12** using iPr$_2$NH and CuI as a base and catalyst, respectively, according to the synthetic procedure for **1** [12]. The mixture of **2**, **14**, and **15** was easily separated and purified by column chromatography.

The synthesis of **3** is shown in Scheme 2. The Ullmann coupling reaction of phenothiazine (**16**) with diiodobiphenyl **8** gave **17**, which was converted to **19** by procedures similar to those from **9** to **11**. Reaction of **13** with an equimolar mixture of acetylenes (**12**:**19** = 1:1) in the presence of excess iPr$_2$NH and a catalytic amount of CuI produced the desired coupling product (**3**) with **15** and **20**.

Absorption and emission of PTZ–Pt–MNDIs (**2** and **3**)

Figure 1a, b shows the absorption spectra of **2** and **3**, respectively, in toluene, and those of reference compounds (Scheme 3). The absorption of these triads in the visible region is attributed to the platinum complex moiety. The PTZ and MNDI moieties had no strong absorption band at wavelengths longer than 400 nm. The

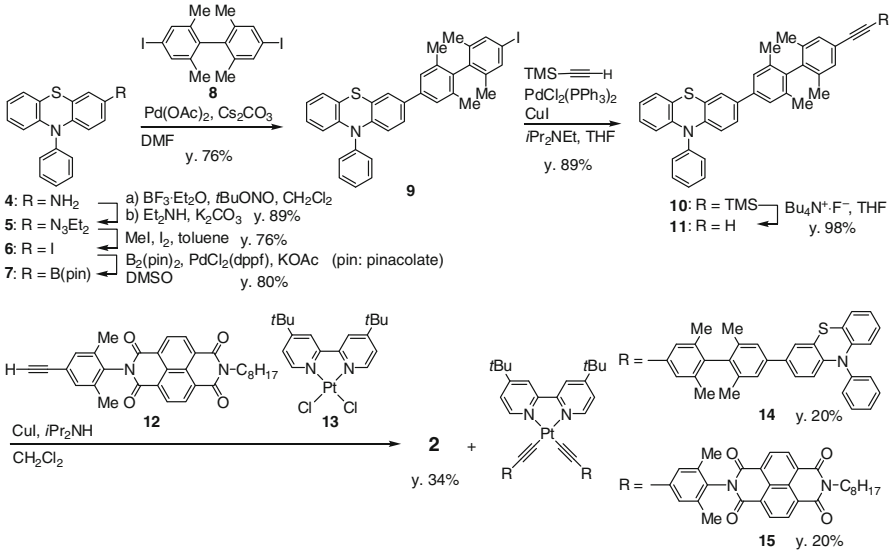

Scheme 1 Synthetic procedures for **2**

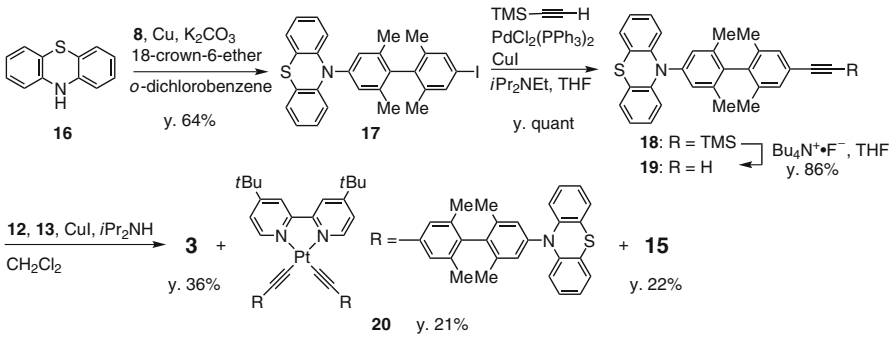

Scheme 2 Synthetic procedures for **3**

absorption bands at ~380 nm are assigned to the π–π^* transition in the MNDI moiety. Absorption of 3PTZ acetylene **11** (λ_{max} = 339 nm) occurs at a longer wavelength than that of 10PTZ acetylene **19** (λ_{max} = 320 nm), which is indicative of the more extended electron delocalization in **11**. The PTZ absorption overlaps with that of the MNDI moiety. The absorption of both triads is almost superimposable with the summation of the spectra of their components (i.e., PTZ, MNDI, and Pt), which suggests negligible electronic interaction between these components in the ground state. Laser light at 532 nm, which selectively excites the Pt complex moiety, was used for picosecond and nanosecond laser photolysis.

The phosphorescence spectra of **2** and **3** in toluene are shown in the insets of Fig. 1a, b, respectively, together with that of reference compound **21**. **21** phosphoresced strongly (λ_{em} = 574 nm) at room temperature in toluene under deaerated conditions. The intensities of the phosphorescence of **2** and **3** are significantly weaker than that of **21**. The efficient quenching of the phosphorescence in **2** and **3** indicates rapid intramolecular electron (or hole) transfer or energy transfer from ^{3}Pt*.

Molecular geometry and molecular orbital calculations for model compounds **2M** and **3M**

The molecular structure of neutral phenothiazine is not planar but rather takes a folded butterfly form [19, 20]. In addition, rotational isomers around acetylenic bonds [12] are possible. Therefore, several conformational isomers of **2** and **3** are likely to exist. We carried out geometrical optimization using MOPAC 2009 (PM6) [16]. Model compounds **2M** and **3M**, in which, for simplicity, methyl groups were used instead of the *tert*-butyl groups on bipyridine and the *n*-octyl group on MNDI, were used in the geometrical optimization and molecular orbital calculations for **2** and **3**. Figure 2 depicts the optimized molecular structures and their highest molecular orbitals (HOMOs) and lowest unoccupied molecular orbitals (LUMOs) for the most stable conformer. The HOMOs and LUMOs are located on the PTZ and MNDI moieties, respectively, in each case. We also compared the MO coefficients of the C_A carbon atom of the twisted biphenylene moiety (optimized structure in

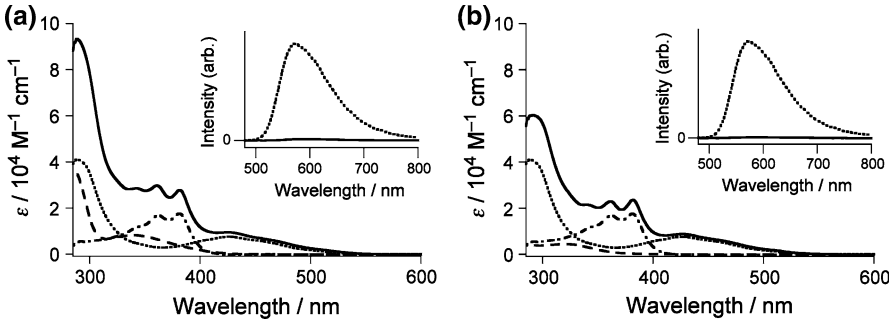

Fig. 1 UV–visible and phosphorescence (*inset*) spectra in toluene: (**a**) for **2** (*solid line*) and (**b**) for **3** (*solid line*), with the spectra of the reference compounds: platinum complex **21** (*dotted line*), naphthalene diimide **12** (*dashed–dotted line*), in both (**a**) and (**b**), phenothiazine **11** (*dashed line*) in (**a**), and phenothiazine **19** (*dashed line*) in (**b**); the phosphorescence spectra are compared at the same absorption intensity at the excitation wavelength of 440 nm

Fig. 2). In **2M**, the C_A carbon atom makes a small but clear contribution to the HOMO. In contrast, the C_A carbon atom in **3M** contributes only slightly (invisible in the HOMO in Fig. 2). The sums of the squares of the HOMO coefficients $\left(\sum c_i^2\right)$ of the C_A carbon are calculated to be 7.1×10^{-3} for **2M** and 1.1×10^{-5} for **3M**. The smaller coefficient of the C_A carbon atom in **3M** is because of the large dihedral angle between the phenothiazine ring and 10-phenyl ring [21]. This difference is discussed further in the section "Nanosecond transient absorption spectra: lifetime of the CS states".

Redox potentials and energy levels of the excited states and the ion pairs of PTZ–Pt–MNDIs

The redox potentials of **2** and **3** were determined by cyclic voltammetry measurements in CH_2Cl_2 (Table 1). Both triads furnished three reversible reduction waves and two reversible or irreversible oxidation waves. The first and second reduction waves are attributed to MNDI (from MNDI to $MNDI^-$ then to $MNDI^{2-}$) whereas the third reduction wave is attributed to the platinum complex (from Pt to Pt^-). The first and second oxidation waves are assigned to PTZ (from PTZ to PTZ^+, from PTZ^+ to PTZ^{2+}). These assignments were made by comparison with the cyclic voltammograms of suitable reference compounds (**9**, **21**, **22**, and **23**). The first

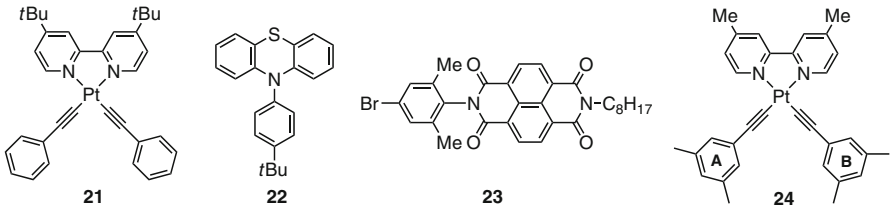

Scheme 3 Chemical formula of **21**, **22**, **23**, and **24**

oxidation wave of **2** was reversible whereas that of **3** was irreversible. PTZs with a terminal acetylene (i.e., **11** and **19**) furnished reversible waves for the first oxidation step. The oxidation potential of the platinum complex was estimated to be +0.59 V from the oxidation peak of **21**. The peaks for Pt → Pt^+ in **2** and **3** appear at +0.92–+1.05 V with the oxidation peak for PTZ^+ → PTZ^{2+}. The higher oxidation potential for the Pt atom in **2** and **3** is probably because of the electron-withdrawing nature of PTZ^+ which destabilizes PTZ^+–Pt^+–MNDI.

Taking these redox potentials into account, the energies for the CS states (E_{CS} in eV) relative to the ground states, in toluene, were estimated by using the Weller approximation (Eq. 1) [22, 23], in which ΔG_S is a correction term for the polarity of the solvent (toluene in this case) (Eq. 2). D and A in these equations represent the donor (i.e., the PTZ or Pt moieties) and the acceptor (i.e., the Pt or MNDI moiety).

$$E_{CS} = e[E_{ox}(D) - E_{red}(A)] + \Delta G_s \quad (1)$$

$$\Delta G_S = \left(e^2/4\pi\varepsilon_0\right) \cdot [(1/2r_D + 1/2r_A) \cdot (1/\varepsilon - 1/\varepsilon_r) - 1/\varepsilon R_{DA}] \quad (2)$$

The CS states are regarded as solvent-separated ion-pairs with a center(+)-to-center(−) distance R_{DA} and effective radii r_D and r_A. ε_0 is the permittivity of a vacuum, and ε and ε_r are, respectively, the relative dielectric constants of the solvent (2.38 for toluene) and reference solvent (8.93 for CH_2Cl_2) in which the redox potentials are measured. We assume that the overall structure of the CS state will not change significantly from that of the neutral state, although the structure of phenothiazine is planar in the radical cation state [21]. From the molecular model calculated at the PM6 level, the estimated distances between donors and acceptors were: $R_{PTZ–MNDI}$ = 21.3 Å, $R_{PTZ–Pt}$ = 16.8 Å, and $R_{Pt–MNDI}$ = 12.4 Å for 3PTZ–Pt–MNDI, and $R_{PTZ–MNDI}$ = 19.2 Å, $R_{PTZ–Pt}$ = 14.7 Å, and $R_{Pt–MNDI}$ = 12.4 Å for

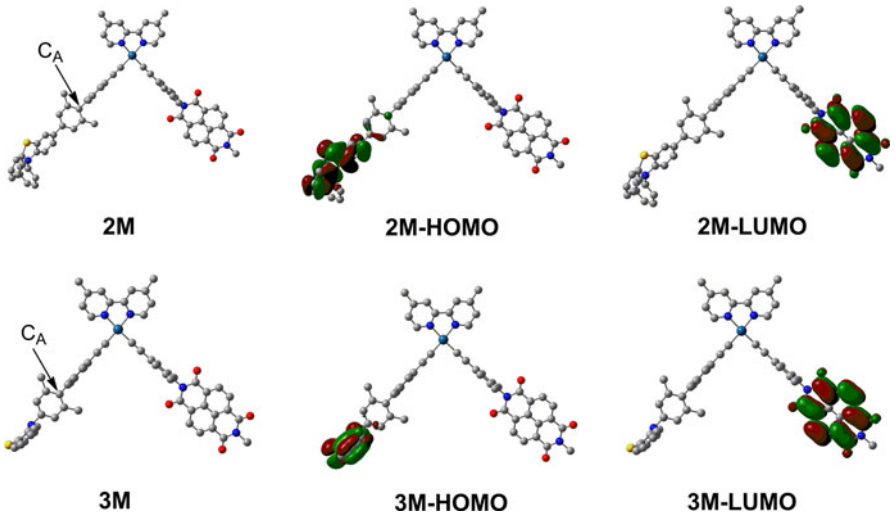

Fig. 2 Optimized structures of **2M** and **3M** and their HOMOs and LUMOs, which were drawn at isovalue = 0.02. **2M** and **3M** denote the model structures for **2** and **3**, respectively (see text). Hydrogen atoms are omitted for clarity

Table 1 Redox potentials of **2** and **3**

Compound	E^{ox2} (V)[a]	E^{ox1} (V)[a]	E^{red1} (V)[a]	E^{red2} (V)[a]	E^{red3} (V)[a]
2	+0.92[b]	+0.21	−1.05	−1.50	−1.86
3	+1.05[b]	+0.25[c]	−1.05	−1.51	−1.88
21	+0.59[b]	–	–	–	−1.86
11	+1.01[b]	+0.25	–	–	–
19	+1.03[b]	+0.26	–	–	–
9	–[c]	+0.23	–	–	–
22	–[c]	+0.26	–	–	–
23	–	–	−1.05	−1.50	–

Measured in CH_2Cl_2 in the presence of 0.1 M tetra-*n*-butylammonium perchlorate as supporting electrolyte

[a] V vs Fc/Fc^+

[b] Irreversible peak potential

[c] Not measured

10PTZ–Pt–MNDI. These values assume that the spin centers are located at the center of the PTZ ring, on the Pt-atom, and at the center of the naphthalene ring. The effective radii were assumed to be $r_{Pt} = r_D = r_A = 4.5$ Å, which is frequently used as a typical value [23, 24].

The energy levels of the partial and full CS states and local excited states are shown in Fig. 3. For both triads, transformation of PTZ–^{3}Pt*–MNDI to the full CS states (PTZ^+–Pt–$MNDI^-$) is exothermic by 0.3 eV. The following path for formation of the full CS state is energetically possible: PTZ–^{3}Pt*–MNDI → PTZ–Pt^+–$MNDI^-$ → PTZ^+–Pt–$MNDI^-$. The energy of PTZ–Pt–^{3}MNDI* is slightly higher than those of the full CS states.

Absorption spectra of electrochemically generated phenothiazine radical cation and naphthalene diimide radical anion

To assign the transient absorption we measured the absorption spectra of $\mathbf{9}^+$, $\mathbf{22}^+$, and $\mathbf{23}^-$ generated under electrochemical oxidation or reduction using a thin-layer cell (Fig. 4). For radical cation $\mathbf{9}^+$, which corresponds to $3PTZ^+$, broad absorption was observed up to approximately 1,000 nm, with peaks at 479, 638, 820, and 920 nm (Fig. 4a). For radical cation $\mathbf{22}^+$, which corresponds to $10PTZ^+$, absorption at 517 nm and broad absorption up to approximately 920 nm was observed, with peaks at 783 and 883 nm (Fig. 4b). The absorption of $\mathbf{9}^+$ occurred in the longer wavelength region than that of $\mathbf{22}^+$, suggesting that the 3PTZ radical cation is more delocalized because of conjugation with the attached phenylene ring. This consideration is compatible with the results of MO calculations, which reveal that the C_A carbon atom in **2** has a larger HOMO coefficient than that in **3**. Radical anion $\mathbf{23}^-$ (i.e., $MNDI^-$) has strong absorption at 473 nm and weak absorption at 606, 690, and 768 nm (Fig. 4c). The molar absorptivity (ε) values of these radical ions are

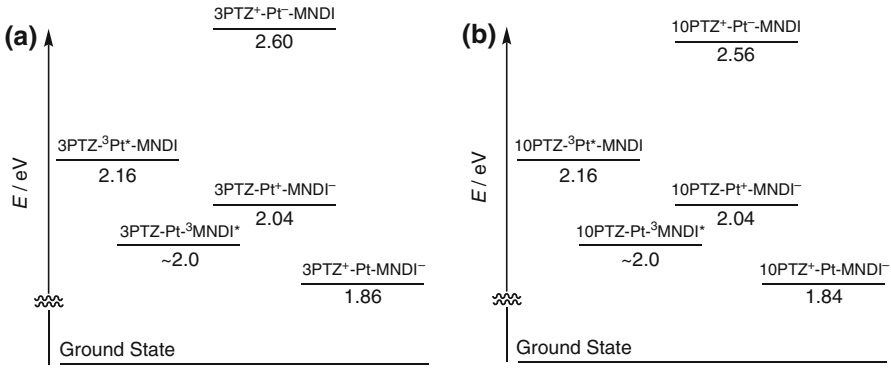

Fig. 3 The energy levels of excited states and CS states for **2** (**a**) and for **3** (**b**)

approximate and assume clean conversion from the neutral species. The ε value at the maximum absorption of $MNDI^-$ is significantly larger than those of the PTZ^+s.

Picosecond transient absorption spectra: formation of the CS states

Picosecond laser photolysis was performed with excitation at 532 nm (FWHM: 17 ps), which selectively excites the Pt-complex chromophore. Figure 5a, b shows the time-resolved difference absorption spectra for **2** and **3**, respectively. Immediately after the laser pulse (0 ps), broad absorption appears in the 550–800 nm region for both **2** and **3**. According to our previous study [12], this absorption is assigned to the ^{3}Pt* state. The ^{3}Pt* absorption is replaced, during 100–1,000 ps, by sharper absorption at 470, ~610, ~690, and ~780 nm for excitation of **2** (Fig. 5a). Similar spectral changes were observed for excitation of **3** (Fig. 5b). In both spectra, the sharp absorption at 470 and 610 nm is clearly assigned to $MNDI^-$ by comparison with the spectra in the electrochemical reduction of **23** (Fig. 4c). The absorption of $3PTZ^+$ (from **2**) and $10PTZ^+$ (from **3**) is ambiguous because it is small and slightly broad (Fig. 4a, b) and overlaps with the larger and sharper absorption of $MNDI^-$. The spectra observed 1 ns after the laser pulse are indicative

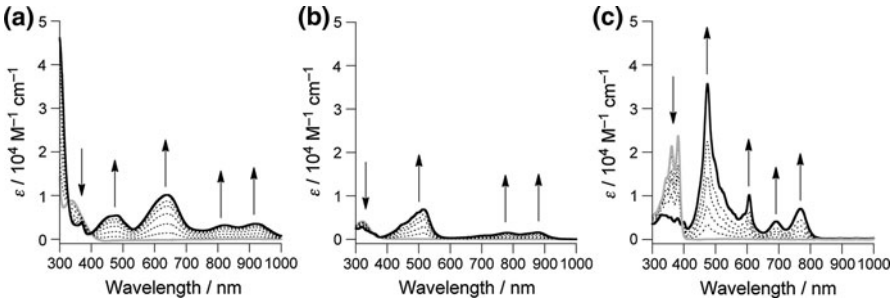

Fig. 4 UV–visible spectra of the electrochemically generated radical cation $\mathbf{9}^+$ (**a**) and of $\mathbf{22}^+$ (**b**), and of radical anion $\mathbf{23}^-$ (**c**). The *gray solid*, *dotted*, and *black* lines show the initial, intermediate, and final states, respectively

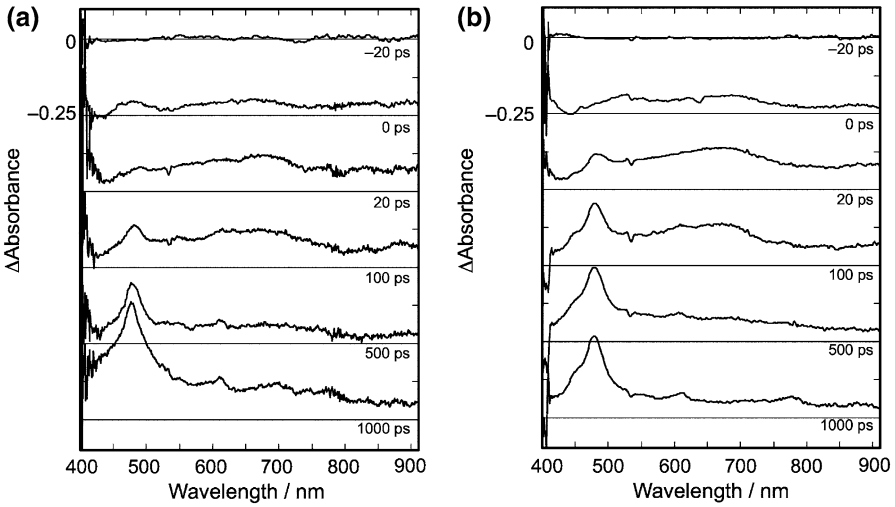

Fig. 5 Picosecond transient difference absorption spectra for **2** (**a**) and **3** (**b**) in toluene under 532 nm laser excitation (FWHM: 17 ps) at room temperature using a 1-mm cell

of the formation the CS states (i.e., $3PTZ^{+}$–Pt–$MNDI^{-}$ and $10PTZ^{+}$–Pt–$MNDI^{-}$). The decay of $^{3}Pt^{*}$ does not differ significantly between **2** and **3** as both have time constants of 200–400 ps. The CS time constants were determined to be 280 ps ($k_{CS} = 3.6 \times 10^{-9}\ s^{-1}$) for **2** and 230 ps ($k_{CS} = 4.4 \times 10^{-9}\ s^{-1}$) for **3**. The quantum yields (Φ) for the formation CS states were estimated to be $\Phi > 0.9$ for both **2** and **3**.[1] These rate constants and quantum yields are similar to those of compound **1** [12]. The phosphorescence time-profile for **2** and **3** at room temperature under nitrogen had comparable lifetimes: 280 ps for **2** and 230 ps for **3**.

Nanosecond transient absorption spectra: lifetime of the CS states

Figure 6 shows the nanosecond transient absorption of **2** and **3** in toluene with laser excitation at 532 nm (FWHM: 4 ns). Nanosecond photolysis produced sharp absorption at 470 and 610 nm, assigned to $MNDI^{-}$, which appeared 20 ns after excitation of **2** (Fig. 6a). A similar spectrum was observed for excitation of **3** (Fig. 6b at 50 ns). The absorption in the 600–700 nm region in Fig. 6a at 20 ns is broader than that in Fig. 6b at 50 ns. This difference reflects the overlap between the $MNDI^{-}$ and $3PTZ^{+}$ absorption in Fig. 6a: $3PTZ^{+}$ absorbs at ~638 nm, whereas $10PTZ^{+}$ absorbs at ~517 nm and has no strong absorption at ~650 nm. The spectra observed are thus consistent with those expected for the CS states.

The time constants for the CR process to the ground states (τ_{CR}) were estimated: The decay curve of $3PTZ^{+}$–Pt–$MNDI^{-}$ (from **2**) was best simulated as a biexponential curve: $\tau_{CR1} = 75$ ns (95 %) and $\tau_{CR2} = 285$ ns (5 %), whereas the decay for $10PTZ^{+}$–Pt–$MNDI^{-}$ (from **3**) was simulated as a single exponential:

[1] The quantum yields for the formation of CS states for the excitation of **2** and **3** were estimated by using the relative intensities of $^{3}Pt^{*}$ (650 nm) and $MNDI^{-}$ (470 nm) in the ps-laser photolysis (Fig. 5).

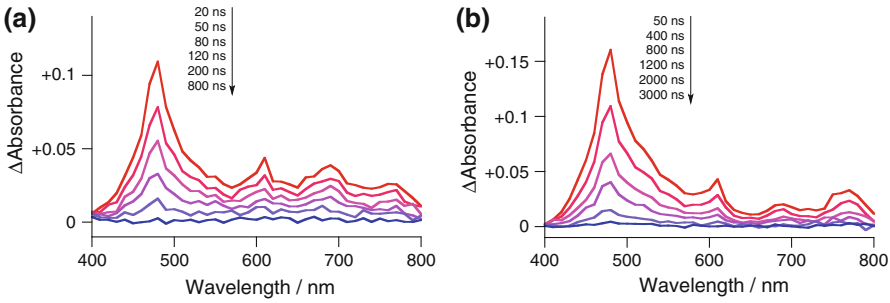

Fig. 6 The nanosecond transient difference absorption spectra of **2** (**a**) and for **3** (**b**) in toluene under 532 nm laser excitation (FWHM: 4 ns) at room temperature using a 10-mm cell

$\tau_{CR} = 830$ ns. The lifetime of 10PTZ$^+$–Pt–MNDI$^-$ was found to be substantially longer than that of 3PTZ$^+$–Pt–MNDI$^-$. The longer lifetime of 10PTZ$^+$–Pt–MNDI$^-$ ($\tau_{CR} = 830$ ns, single exponential in toluene) was nearly identical with that ($\tau_{CR} = 839$ ns, single exponential in toluene) of the CS state from **1** [12].

The origin of the biexponential decay observed for 3PTZ$^+$–Pt–MNDI$^-$ is not clear and may be because of conformational isomers around the acetylenic bonds or around the C–C bond directly connected to the 3PTZ group, as discussed in the previous section.

Mechanistic consideration of the photoinduced CS and CR processes

In principle, two mechanisms for formation of CS state are possible:

1. PTZ–^{3}Pt*–MNDI → PTZ–Pt$^+$–MNDI$^-$ → PTZ$^+$–Pt–MNDI$^-$; and
2. PTZ–^{3}Pt*–MNDI → PTZ–Pt–^{3}MNDI* → PTZ$^+$–Pt–MNDI$^-$.

In our previous study of a related system (i.e., MTA–Pt–MNDI), the radical ions (MTA$^+$ and MNDI$^-$) were observed in different absorption regions. Formation of the radical ions was found to have different time constants, indicative of mechanism 1 [12]. In this case, decay of PTZ–^{3}Pt*–MNDI was shown to be 200–400 ps in the picosecond transient spectra for **2** and **3** (Fig. 5). The phosphorescence of PTZ–^{3}Pt*–MNDI decays with a similar time constant. The absorption of MNDI$^-$ increases with a similar time constant. These results are compatible with mechanism 1. Mechanism 2 involves exothermic energy transfer from PTZ–^{3}Pt*–MNDI to PTZ–Pt–^{3}MNDI* in the 1st step and long-distance electron transfer from PTZ to ^{3}MNDI* in the 2nd step. The rate-determining step is likely to be in the 2nd step. In such a case, PTZ–Pt–^{3}MNDI* is expected to be observed. However, no evidence was obtained for the formation of PTZ–Pt–^{3}MNDI*, therefore, the CS formation for these triads is likely to follow mechanism 1.

The driving forces for the CR process were estimated from the energy levels of PTZ$^+$–Pt–MNDI$^-$ ($\Delta G_{CR} \approx -1.85$ eV for both the 3PTZ and 10PTZ derivatives (Table 2; Fig. 3)). However, the τ_{CR} value of 10PTZ$^+$–Pt–MNDI$^-$ (830 ns) is much longer than those of 3PTZ$^+$–Pt–MNDI$^-$ ($\tau_{CR1} = 75$ ns (95 %) and $\tau_{CR2} = 285$ ns

Table 2 The distances between redox moieties and the energy for the CS states

Compound	R_{D-A} (Å)	R_{Pt-A} (Å)	R_{D-Pt} (Å)	$E_{D^+-A^-}$ (eV)	$E_{Pt^+-A^-}$ (eV)	$E_{D^+-Pt^-}$ (eV)
2	21.3	12.4	16.8	1.86	2.04	2.60
3	19.2	12.4	14.7	1.84	2.05	2.56

(5 %)). The difference between the decay time constants could be because of the electronic coupling matrix element V_{DA}, which is involved in the pre-exponential term in the Marcus theory. 3PTZ$^+$–Pt–MNDI$^-$ (from **2**) would have a larger V_{DA} value than 10PTZ$^+$–Pt–MNDI$^-$ (from **3**). This consideration is supported by the two observations:

1. the C_A atom (see formulas **2** and **3** in Fig. 2) in the twisted biphenyl linker has a larger HOMO coefficient in **2** than in **3**; and
2. **9**$^+$, which is a model of 3PTZ$^+$ from **2**, has an absorption maximum at a longer wavelength than **22**$^+$, which is a model of 10PTZ$^+$ from **3**.

The larger V_{DA} value in 3PTZ$^+$–Pt–MNDI$^-$ may affect the CS process and the CR process. However, the CS time constants of **2** and **3** are not significantly different in the picosecond transient absorption. A larger electronic effect on the CR process than on the CS process has frequently been observed for several related dyads [25, 26].

In our previous report on MTA–Pt–MNDI [12], the CS state was demonstrated to be in a SCRP state. Although time-resolved electron paramagnetic resonance (TREPR) studies were not carried out in this study, it is very likely that this system also proceeds via an SCRP state. The SCRP state is an equilibrium state between singlet–triplet mixed states, $^{T'}$(PTZ$^+$–Pt–MNDI$^-$) and $^{S'}$(PTZ$^+$–Pt–MNDI)$^-$ (the superscripts S′ and T′ denote singlet-predominant and triplet-predominant states, respectively), at zero magnetic field. The relatively long lifetime observed for the CS state (especially for **3**) reflects not only the electronic interaction V_{DA} but also the spin-state differences between the SCRP and the ground states. The observed lifetimes of the CS states also depend on the rate of intersystem crossing in these radical pairs [27–30, and references cited therein]. Further studies to elucidate the mechanism of the spin-sorted charge recombination are in progress.

Conclusion

We prepared two triads, 3PTZ–Pt–MNDI (**2**) and 10PTZ–Pt–MNDI (**3**). The CS state formation and decay were studied in toluene using picosecond and nanosecond laser photolysis with selective excitation of the Pt-moiety. Formation of the CS states, PTZ$^+$–Pt–MNDI$^-$ from PTZ–^{3}Pt*–MNDI, was observed to have similar time constants: $\tau_{CS} = 280$ ps for 3PTZ$^+$–Pt–MNDI$^-$ and $\tau_{CS} = 230$ ps for 10PTZ$^+$–Pt–MNDI$^-$. However, the lifetimes of the CS states were found to be very different: $\tau_{CR1} = 75$ ns (95 %) and $\tau_{CR2} = 285$ ns (5 %) for 3PTZ$^+$–Pt–MNDI$^-$ and

$\tau_{CR} = 830$ ns for $10PTZ^{+}$–Pt–$MNDI^{-}$. The longer lifetime of the CS state of $10PTZ^{+}$–Pt–$MNDI^{-}$ (from **3**) suggests the importance of the electronic coupling matrix element V_{DA} and the spin-state difference between the possible SCRP state and the ground state.

Acknowledgments This work was supported by Grants-in-Aid: for Scientific Research (B) (no. 2350066 for K.O.), for Young Scientists (B) (no. 22750043 for S.S.), and for JSPS Fellows (no. 238419 for R.S.) from the Japan Society for Promotion of Science (JSPS). S.S. is also grateful for financial support from the Kansai Research Foundation for Technology Promotion and the Association for the Progress of New Chemistry.

References

1. K.E. McAuley, P.K. Fyfe, J.P. Ridge, N.W. Isaacs, R.J. Cogdell, M.R. Jones, Proc. Natl. Acad. Sci. USA **96**, 14706–14711 (1999)
2. G.J. Kavarnos, *Fundamentals of Photoinduced Electron Transfer* (Wiley, New York, 1993)
3. J.W. Verhoeven, J. Photochem. Photobiol. C **7**, 40–60 (2006)
4. M. Borgström, N. Shaikh, O. Johansson, M.F. Anderlund, S. Styring, B. Åkermark, A. Magnuson, L. Hammarström, J. Am. Chem. Soc. **127**, 17504–17515 (2005)
5. L. Flamigni, J.-P. Collin, J.-P. Sauvage, Acc. Chem. Res. **41**, 857–871 (2008)
6. L. Flamigni, E. Baranoff, J.-P. Collin, J.-P. Sauvage, Chem. Eur. J. **12**, 6592–6606 (2006)
7. S. Chakraborty, T.J. Wadas, H. Hester, R. Schmehl, R. Eisenberg, Inorg. Chem. **44**, 6865–6878 (2005)
8. J.E. McGarrah, Y.-J. Kim, M. Hissler, R. Eisenberg, Inorg. Chem. **40**, 4510–4511 (2001)
9. M. Hissler, J.E. McGarrah, W.B. Connick, D.K. Geiger, S.D. Cummings, R. Eisenberg, Coord. Chem. Rev. **208**, 115–137 (2000)
10. S.D. Cummings, R. Eisenberg, J. Am. Chem. Soc. **118**, 1949–1960 (1996)
11. W. Paw, S.D. Cummings, M.A. Mansour, W.B. Connick, D.K. Geiger, R. Eisenberg, Coord. Chem. Rev. **171**, 125–150 (1998)
12. S. Suzuki, R. Sugimura, M. Kozaki, K. Keyaki, K. Nozaki, N. Ikeda, K. Akiyama, K. Okada, J. Am. Chem. Soc. **131**, 10374–10375 (2009)
13. H. Kawauchi, S. Suzuki, M. Kozaki, K. Okada, D.-M.S. Islam, Y. Araki, O. Ito, K. Yamanaka, J. Phys. Chem. A **112**, 5878–5884 (2008)
14. Y. Nomura, Y. Takeuchi, J. Chem. Soc. B 956–960 (1970)
15. M. Hissler, W.B. Connick, D.K. Geiger, J.E. McGarrah, D. Lipa, R.J. Lachicotte, R. Eisenberg, Inorg. Chem. **39**, 447–457 (2000)
16. MOPAC2009, J.J.P. Stewart, *Stewart Computational Chemistry*, version 9.211W (2009). http://OpenMOPAC.net, Accessed June 4, 2012
17. T. Ohno, K. Nozaki, M. Haga, Inorg. Chem. **31**, 548–555 (1992)
18. A. Yoshimura, K. Nozaki, N. Ikeda, T. Ohno, J. Phys. Chem. **100**, 1630–1637 (1996)
19. J.J.H. McDowell, Acta. Cryst. **B32**, 5–10 (1976)
20. C.L. Klein, J.M. Conrad III, S.A. Morris, Acta. Cryst. **C41**, 1202–1204 (1985)
21. T. Okamoto, M. Kuratsu, M. Kozaki, K. Hirotsu, A. Ichimura, T. Matsushita, K. Okada, Org. Lett. **6**, 3493–3496 (2004)
22. A.Z. Weller, Phys. Chem. Neue Folge **133**, 93–98 (1982)
23. M. Lor, L. Viaene, R. Pilot, E. Fron, S. Jordens, G. Schweitzer, T. Weil, K. Müllen, J.W. Verhoeven, M. Van der Auweraer, F.C. De Schryver, J. Phys. Chem. B **108**, 10721–10731 (2004)
24. H. Oevering, M.N. Paddon-Row, M. Heppener, A.M. Oliver, E. Cotsaris, J.W. Verhoeven, N.S. Hush, J. Am. Chem. Soc. **109**, 3258–3269 (1987)
25. A.L. Thompson, T.-S. Ahn, K.R.J. Thomas, S. Thayumanavan, T. Martínez, C.J. Bardeen, J. Am. Chem. Soc. **127**, 16348–16349 (2005)
26. A.B. Ricks, G.C. Solomon, M.T. Colvin, A.M. Scott, K. Chen, M.A. Ratner, M.R. Wasielewski, J. Am. Chem. Soc. **132**, 15427–15434 (2010)
27. G.L. Closs, M.D.E. Forbes, J.R. Jr. Norris, J. Phys. Chem. **91**, 3592–3599 (1987)

28. P.J. Hore, in *Advanced EPR in Biology and Biochemistry*, ed. by A.J. Hoff (Elsevier, Amsterdam, 1989), pp. 405–440
29. Z.E.X. Dance, Q. Mi, D.W. McCamant, M.J. Ahrens, M.A. Ratner, M.R. Wasielewski, J. Phys. Chem. B **110**, 25163–25173 (2006)
30. T. Miura, A.M. Scott, M.R. Wasielewski, J. Phys. Chem. C **114**, 20370–20379 (2010)